ACS OMEGA

Open Access

This article is licensed under CC-BY-NC-ND 4.0

http://pubs.acs.org/journal/acsodf

Article

3D-Printed Composite Bioceramic Scaffolds for Bone and Cartilage Integrated Regeneration

Nanjian Xu,◆ Dezhi Lu,◆ Lei Qiang,◆ Yihao Liu, Dalin Yin, Zhiyong Wang, Yongxiang Luo, Chen Yang, Zhenjiang Ma,* Hui Ma,* and Jinwu Wang*

Cite This: *ACS Omega* 2023, 8, 37918−37926

Read Online

ACCESS | Metrics & More | Article Recommendations

ABSTRACT: Osteoarthritis may result in both cartilage and subchondral bone damage. It is a significant challenge to simultaneously repair cartilage due to the distinct biological properties between cartilage and bone. Here, strontium copper tetrasilicate/β-tricalcium phosphate (Wesselsite-$[SrCuSi_4O_{10}]/Ca_3(PO_4)_2$, WES-TCP) composite scaffolds with different WES contents (1, 2, and 4 wt %) were fabricated via a three-dimensional (3D) printing method for the osteochondral regeneration. The physicochemical properties and biological activities of the scaffolds were systematically investigated. 2WES-TCP (WES-TCP with 2 wt % WES) composite scaffolds not only improved the compressive strength but also enhanced the proliferation of both rabbit bone mesenchymal stem cells (rBMSCs) and chondrocytes, as well as their differentiation. The in vivo study further confirmed that WES-TCP scaffolds significantly promoted the regeneration of both bone and cartilage tissue in rabbit osteochondral defects compared with pure TCP scaffolds owing to the sustained and controlled release of bioactive ions (Si, Cu, and Sr) from bioactive scaffolds. These results show that 3D-printed WES-TCP scaffolds with bilineage bioactivities take full advantage of the bifunctional properties of bioceramics to reconstruct the complex osteochondral interface, which broadens the approach to engineering therapeutic platforms for biomedical applications.

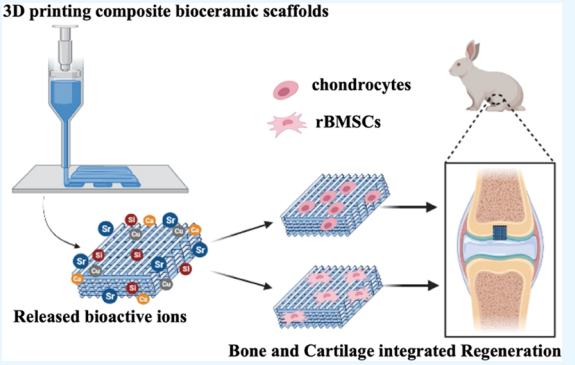

1. INTRODUCTION

Osteoarthritis (OA) is a degenerative disease that involves damage to articular cartilage and the underlying subchondral bone. The loss of tissue leads to a large defect, causing pain during movement.[1] Due to significant joint pain and limited joint mobility, the daily activities of 500 million people (7% of the global population) are severely affected.[2] Current treatment strategies for OA are still problematic within the clinical setting because of subchondral bone structural remodeling and articular hyaline cartilage degradation.[3] According to the special biological microstructure of subchondral bone and articular cartilage, it is a significant challenge to construct a bioactive scaffold with the ability to simultaneously repair the osteochondral tissue defect in tissue engineering.

The properties of bone and cartilage are different from each other because of their specific anatomic function and structure. Mechanically, the compressive modulus diminishes from bone to cartilage. Biochemically, water concentration and collagen diminish from cartilage to osseous tissue, while mineral content increases.[4] As is known, auto/allograft is a golden standard for osteochondral regeneration.[5] However, there are some limitations, such as insufficient donator, secondary injury, and immune rejection. Although different kinds of artificial bone implants have been prepared to attempt to overcome the challenge, such as polymers (poly(D,L-lactic-*co*-glycolic acid), poly(caprolactone), poly(ethylene glycol), poly(glycolic acid), etc.), metallic materials (titanium, titanium alloys, cobalt−chromium alloy, stainless steel, etc.), and inorganic materials (hydroxyapatite, β-tricalcium phosphate, etc).[6] In addition, two-dimensional nanomaterial-functioned PEEK implants exhibited enhanced cytocompatibility, in vivo osseointegration, and bone remodeling ability.[7,8] However, there are a few biomaterials that have the ability to induce the regeneration of both cartilage and subchondral. With the development of tissue engineering, osteochondral tissue engineering has emerged and brought new hopes for osteochondral defect repair.

The reconstruction of the osteochondral matrix microenvironment is key to cartilage regeneration, and bioactive material scaffold provides an appropriate microenvironment for the regeneration of subchondral bone and cartilage tissues.[9]

Received: May 11, 2023
Accepted: September 4, 2023
Published: October 2, 2023

ACS Publications

© 2023 The Authors. Published by American Chemical Society

However, the three-dimensional (3D) printed monophasic scaffold is limited by biological and mechanical properties and cannot achieve cartilage and subchondral tissue regeneration.[10] Although the 3D-printed multiphasic scaffolds can mimic the construction of subchondral tissues and cartilage, it is incompetent to biologically mimic the stability and integrity of the subchondral bone and cartilage due to the complex properties and microstructure of the bone−cartilage interface.[1] In addition, the bonding strength between the two adjacent phases is often insufficient, resulting in the separation of the layers. Therefore, it is important to design and fabricate a bioactive scaffold that possesses a dual-functional scaffold for simultaneously regenerating bone and cartilage.

Strontium copper tetrasilicate (WES, $SrCuSi_4O_{10}$,) belongs to the "Egyptian Blue Family" and exhibits high biocompatibility both in vitro and in vivo.[11] Sr is one of the alkali metals and is an essential trace icon in the human body. It has attracted the attention of scholars that 99.1% of absorbed Sr element is deposited in human bones and teeth, especially newly formed bones.[12,13] Some studies have indicated that the "dual regulation" of Sr is highly related to bone metabolism, it can inhibit osteoclast activity for reducing bone resorption while stimulating osteoblasts to secrete bone matrix.[14−16] Recent studies demonstrated that the released Cu and Si ions from $CaCuSi_4O_{10}$ could boost vascular endothelial to express hypoxia-inducible factor-1 and growth factor for stimulating new blood vessel formation.[17,18] It has been proved that the released bioactive ions (Si and Sr) from biomaterial scaffolds are powerful elements for osteogenesis.[19] Therefore, composite bioceramic scaffolds may have significant potential for the simultaneous regeneration of subchondral and cartilage tissues.

In this work, a 3D-printed composite scaffold was designed and fabricated by the addition of WES into β-TCP bioceramics. Such 3D-printed bioactive composite scaffolds are expected for regenerating subchondral and cartilage tissues attributed to the sustained release of bioactive ions. The incorporation of WES into β-TCP improved the compressive strength of the composite bioactive scaffolds. 3D-printed bioceramic WES-TCP scaffolds with bilineage bioactivities significantly enhanced the proliferation of rabbit bone mesenchymal stem cells (rBMSCs) and chondrocytes and improved their differentiation. Furthermore, the composite scaffolds obviously promoted the formation of bone tissue and cartilage tissue in vivo. Therefore, the prepared composite scaffolds represent an intelligent strategy for osteochondral tissue regeneration.

2. MATERIALS AND METHODS

2.1. Materials. Copper carbonate ($CuCO_3$), strontium carbonate ($SrCO_3$), and silicon dioxide (SiO_2) were purchased from Aladdin Reagent Co., Ltd. (Shanghai, China). Pluronic F-127 (20 wt %) was obtained from Sigma-Aldrich, and TCP ceramics were purchased from Kunshan Chinese Technology New Materials Co., Ltd. (Jiangsu, China).

2.2. Fabrication and Characterization of WES-TCP Scaffolds. Briefly, we use a simple solid-state reaction method to synthesize WES powders.[20] The mixed powders of 1×10^{-3} m $CuCO_3$, 1×10^{-3} m $SrCO_3$, and 4×10^{-3} m SiO_2 were ground in a pestle mortar until homogeneous and heated at 1000 °C for 16 h in a platinum crucible with a heating rate of 5 °C min^{-1}. The obtained products were regrounded and heated by the same sintering condition. The unreacted raw materials are removed by excess HCl solution (1 M). The WES-TCP scaffolds were manufactured by the 3D plotting device (BioScaffolder 3.1, Gesim, Germany) with a computer-assisted design (CAD) model. We mixed 1, 2, and 4 wt % of WES and TCP powders respectively, then added 20 wt % F-127 (Poloxamer) to the mixture, and stirred until it became homogeneous. Then, the primary scaffold was fabricated by extruding the ink through nozzles (needle standard: 22 G). The dosing pressure was 1.5−2.5 bar, and the speed of the plotting head was 6 mm s^{-1}. WES-TCP scaffolds of 10 mm × 10 mm × 1.5 mm following a crossed lay-dawn pattern (45°) were prepared and photographed. As a control, pure TCP scaffolds were also 3D printed using the same protocol.

To obtain WES-TCP scaffolds, the primary scaffolds were dried overnight at room temperature. The WES-TCP scaffolds were sintered at 1100 °C for 3 h, and the heating rate was 2 °C min^{-1}. The TCP scaffolds were prepared using the same method as controls.

The compositions of TCP scaffolds with different WES were evaluated by an X-ray diffractometer (XRD) using Cu Kα radiation and operating at 40 kV with 40 mA current. Macrophotograph and surface morphology of SPS scaffolds were obtained from an optical camera and a scanning electron microscope (FEI APREO S, Thermo Scientific, Netherland), respectively. A static mechanical test machine (INSTRON 5566, Germany) was used for mechanical testing, and the composite scaffolds were tested under a constant displacement rate of 1.0 mm min^{-1}.

To evaluate the degradation of WES-TCP scaffolds, they were soaked in Tris−HCl (pH 7.4) in a 37 °C shaking water bath for 1, 7, 14, 21, and 28 d, respectively. The ratio of Tris−HCl volume to composite scaffold mass was 200 mL g^{-1}. The average ionic concentrations of Sr, Si, and Cu elements within the Tris−HCl solutions were measured using inductively coupled plasma atomic emission spectroscopy (ICPAES; Varian). After the set soaking time, the composite scaffolds were dried overnight at 60 °C, and the final weight of every scaffold was accurately measured. The weight loss was expressed as a percentage of the initial weight of the composite scaffolds.

2.3. Cell Culture Experiments with rBMSCs and Chondrocytes. Rabbit chondrocytes were provided by Prof. Wang from Ninth People's Hospital Affiliated to Shanghai Jiaotong University School of Medicine, and they were cultivated in Dulbecco's modified Eagle's medium low-glucose (Thermo Fisher Scientific, Grand Island, America) containing 10% fetal calf serum (Thermo Fisher Scientific), 100 μg mL^{-1} streptomycin, and 100 μ mL^{-1} penicillin (Thermo Fisher Scientific) at 5% CO_2 and 37 °C. The rabbit rBMSCs were cultivated in mesenchymal stem cell basal medium containing 10% rabbit mesenchymal stem cell-qualified fetal bovine serum, 100 μg mL^{-1} streptomycin, 100 μ mL^{-1} penicillin, and glutamine at 5% CO_2 and 37 °C. The above reagents were purchased from Gibco.

2.4. Cell Proliferation Assay. rBMSCs with a density of 1 × 10^5 cells per well were seeded on (1, 2, 4)WES-TCP scaffolds and TCP for control in 24-well plates and cultured at 5% CO_2 and 37 °C for 1, 4, and 7 days. At each set time, the original medium was refused, and every well was rinsed by PBS three times. Then, rBMSCs were incubated in a 10% CCK-8 (Dojindo, Kumamoto, Japan) solution at 37 °C for 1.5 h. Subsequently, the cell viability was assessed by detecting the optical density at 450 nm. The chondrocytes were tested with the same method.

https://doi.org/10.1021/acsomega.3c03284
ACS Omega 2023, 8, 37918−37926

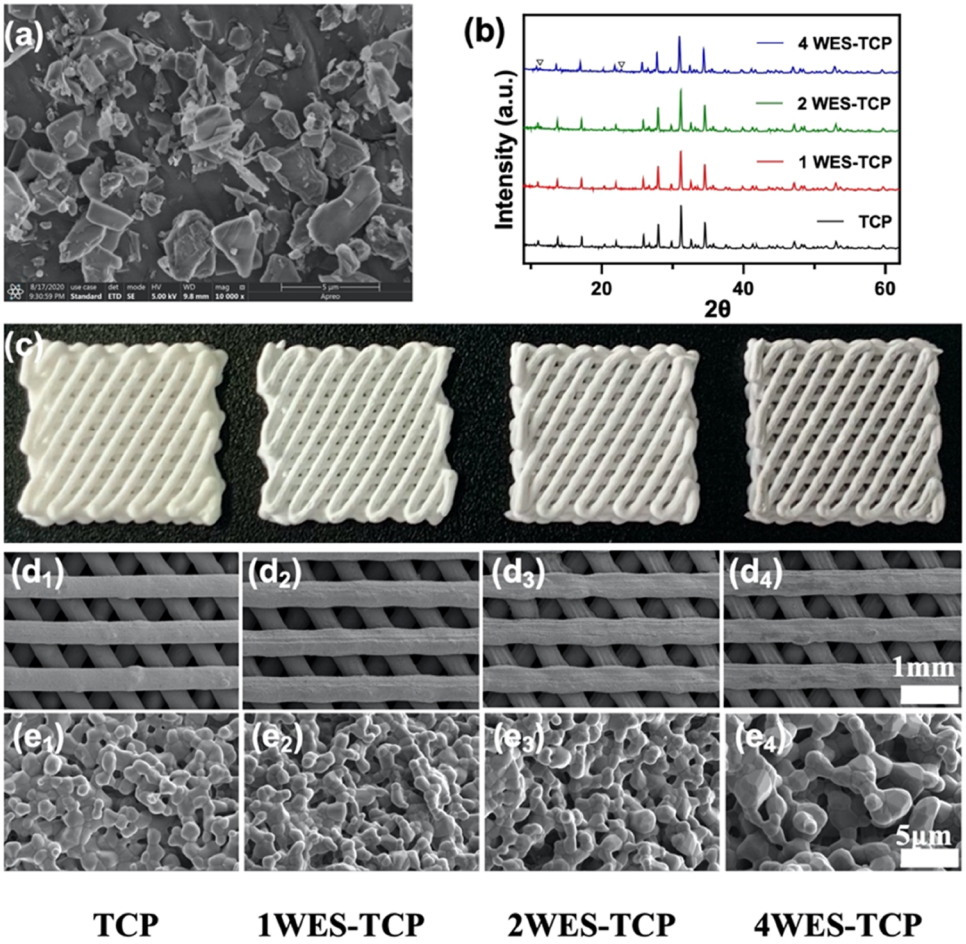

Figure 1. Preparation of 3D-printed WES-TCP scaffolds. SEM image of the WES powders (a). XRD patterns of TCP and (1, 2, 4)WES-TCP calcined at 1100 °C (b). Photographs of 3D-printed TCP and WES-TCP composite scaffolds (c). SEM images of TCP (d_1, e_1), 1WES-TCP(d_2, e_2), 2WES-TCP(d_3, e_3), and 4WES-TCP(d_4, e_4) scaffolds with different magnifications. WES-TCP composite scaffolds with a uniform macrostructure were successfully fabricated via the 3D printing method.

2.5. Quantitative Real-Time Reverse-Transcriptase Polymerase Chain Reaction. An RNAprep Micro Kit (TaKaRa, Japan) was used to evaluate the mRNA transcript levels of osteogenic specific genes (SP7, OCN, and Runx-2) and chondrocytes specific genes (COL II, AGGRECAN, and SOX-9) at 7 d. The Prime Script first Strand cDNA synthesis kit (TOYOBO, Japan) was used to prepare cDNA, and the multifunction microplate reader (SpectraFluor Plus, Tecan, Crailsheim, Germany) was used to determine the concentration of RNA at 260 nm. Cycle conditions were as follows: reverse transcription at 60 °C for 20 min; activation of HotStarTaq DNA polymerase/inactivation of reverse transcriptase at 95 °C for 1 min; and 40 cycles of 95 °C for 15 s and 72 °C for 45 s. All of the primer sequences (Invitrogen Inc., Carlsbad, CA) were designed with primer 5.0 software.

2.6. In Vivo Regeneration of Cartilage and Bone for WES-TCP Scaffolds. The in vivo experiments were performed according to the guidelines authorized by the Ninth People's Hospital Affiliated with the Shanghai Jiaotong University School of Medicine Ethics Committee (No. SH9H-2021-A607-SB). To evaluate the regeneration effect of pure TCP and 2WES-TCP scaffolds, the osteochondral defect model (height: 5 mm, diameter: 4 mm) was created on the groove of knees in eligible rabbits (3 months old, 2−2.5 kg). Then, the 2WES-TCP or TCP scaffolds were implanted into the defects, respectively, and the control group was Blank control. The knee joints of the rabbits were collected for gross observation and histological analysis at 12 weeks postsurgery. The histological analysis was performed to observe the formation of bone and cartilage tissues in the defect sites. All tissue samples were hydrated, embedded in PMMA, and sliced. After being polished, the tissue sections were stained with Van Gieson (V&G) and Toluidine blue dyes. Finally, the staining images were observed via a microscope.

2.7. Statistical Analysis. The experimental data were expressed as mean ± standard deviation (SD) and analyzed by one-way analysis of variance (ANOVA) with a post-hoc test. A value of $p < 0.05$ was considered statistically significant and the data were indicated with (*) for probability less than 0.05 ($p < 0.05$), (**) for $p < 0.01$, (***) for $p < 0.001$, and (****) for $p < 0.0001$.

3. RESULTS

3.1. Characterization and Fabrication of 3D-Printed WES-TCP Composite Scaffolds. The morphology of the developed WES powders is shown in Figure 1a. The X-ray diffractometer (XRD) patterns of pure TCP and WES (1, 2, 4)-TCP sintered under different temperatures are shown in Figure 1b. The pure TCP and WES-TCP composite scaffolds (denoted as 1WES-TCP, 2WES-TCP, 4WES-TCP) were

https://doi.org/10.1021/acsomega.3c03284
ACS Omega 2023, 8, 37918−37926

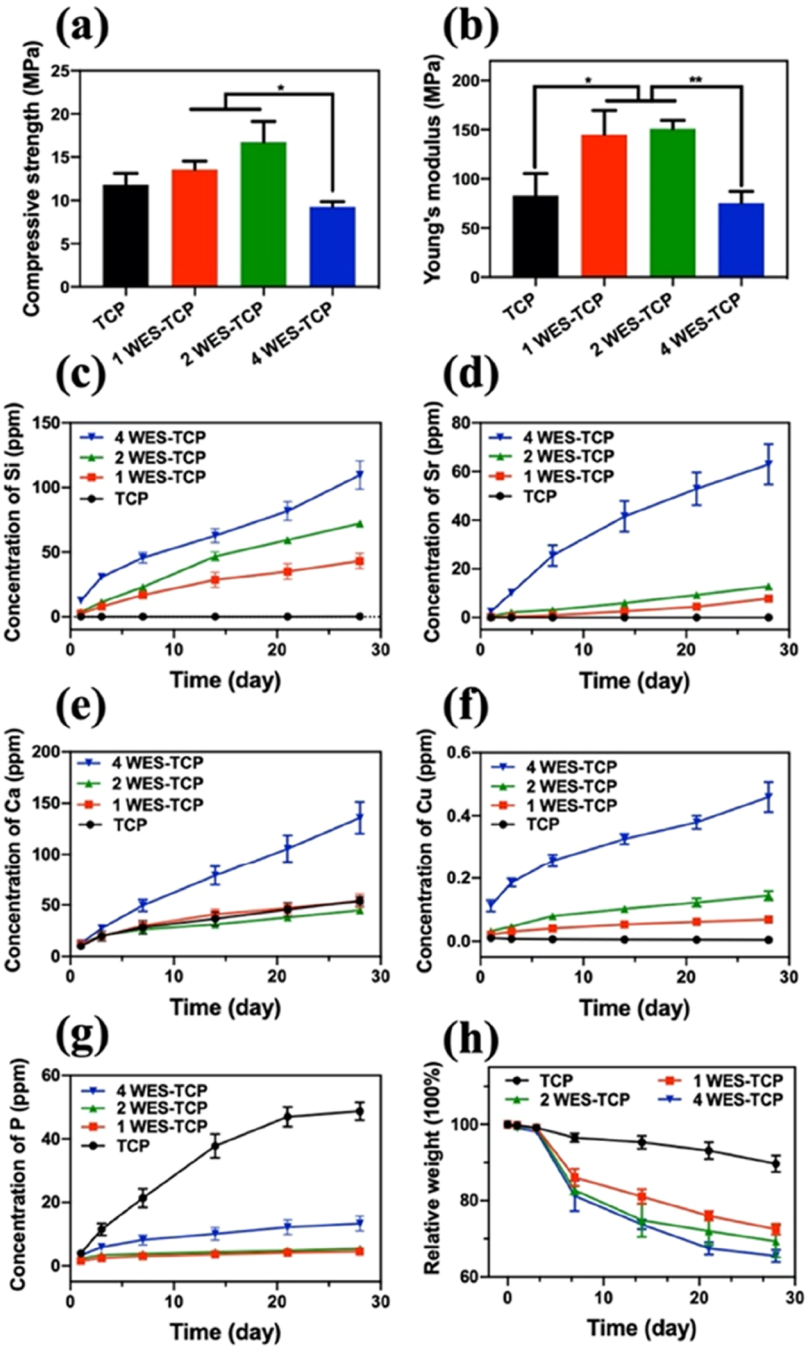

Figure 2. Characterizations of TCP and (1, 2, 4)WES-TCP scaffolds. Compressive strength of TCP and (1, 2, 4)WES-TCP scaffolds (a). Compressive Young's moduli of TCP and (1, 2, 4)WES-TCP scaffolds (b). Concentration of released Si (c), Sr (d), Ca (e), Cu (f), and P (g) elements from the composite scaffolds. Degradation behavior of TCP and (1, 2, 4)WES-TCP scaffolds in the Tris−HCl solution (pH 7.4) (h).

fabricated through extrusion-based 3D printing techniques. The photographs of 3D-printed scaffolds are shown in Figure 1c. All of the scaffolds possessed smooth surfaces with uniform 45° interlaced architectures. As shown in the scanning electron microscopy (SEM) images in Figure 1d,1e, the obtained 3D-printed scaffolds had a controllable macrostructure, and the surface morphologies of TCP, 1WES-TCP, and 2WES-TCP were denser than that of 4WES-TCP.

As shown in Figure 2a, the results of the mechanical property analysis showed that the compressive strength of 2WES-TCP was obviously higher than those of other scaffolds, and the average compressive strength of TCP and (1, 2, and 4)WES-TCP scaffolds was 11.82, 13.58, 16.78, and 9.26 MPa, respectively. As shown in Figure 2b, compared to pure TCP scaffolds, the incorporation of the WES improved the compressive Young's moduli of 3D-printed WES-TCP scaffolds, and the 2WES-TCP group exhibited the highest Young's modulus of 151.03 ± 8.59 MPa. There was no significant difference in the compressive Young's moduli between those of pure TCP and 4WES-TCP scaffolds.

The sustained release of bioactive elements (Si, Sr, Ca, Cu, and P) from 3D-printed TCP and WES-TCP composite scaffolds was detected (Figure 2c−g). The release profiles stand for the average rates of bioactive ions released at each

https://doi.org/10.1021/acsomega.3c03284
ACS Omega 2023, 8, 37918−37926

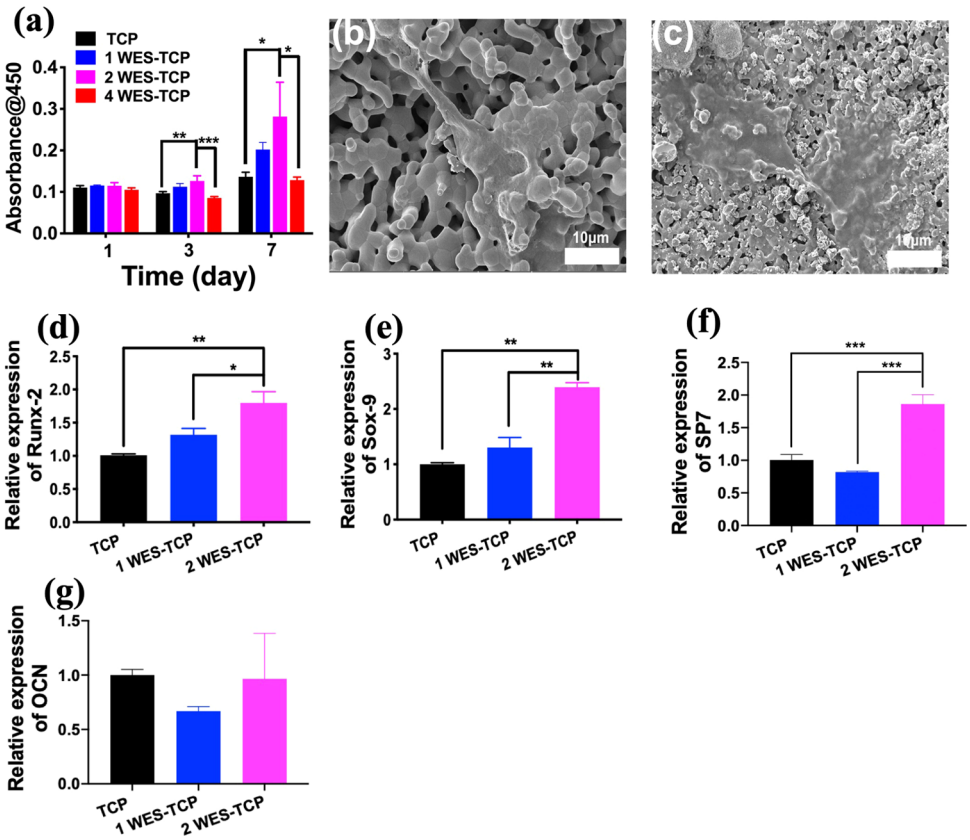

Figure 3. Proliferation and morphology of rBMSCs cultured on 3D-printed TCP and WES-TCP scaffolds. Proliferation of rBMSCs cultured on pure TCP and WES-TCP scaffolds (a). SEM images of rBMSCs after seeding on TCP (b) and 2WES-TCP (c) scaffolds. The gene expression of Runx-2 (d), Sox-9 (e), SP7 (f), and OCN (g) in rBMSCs after coculturing with scaffolds for 7 d ($n = 3$, *$p < 0.05$, **$p < 0.01$, ***$p < 0.001$, ****$p < 0.0001$).

time point. Compared to pure TCP and (1, 2)WES-TCP scaffolds, the bioactive Si, Sr, Ca, and Cu ions of 4WES-TCP scaffolds exhibited a much higher ionic release during 4 weeks. As shown in Figure 2h, the results of degradation profiles displayed a decreasing trend of the relative weight, and the average weight loss of pure TCP and (1, 2, 4)WES-TCP scaffolds immersed in the Tris−HCl solution for 28 days was 10.31, 27.47, 30.67, and 34.46%, respectively. Previous studies have shown that the release of Cu, Si, and Sr ions plays a significant role in osteogenesis.[21] Thus, the degradation of 3D-printed WES-TCP composite scaffolds is expected to enhance bone regeneration.

3.2. WES-TCP Composite Scaffolds Stimulating the Proliferation and Differentiation of rBMSCs. The in vitro osteogenic performance of 3D-printed pure TCP and (1, 2, 4)WES-TCP composite scaffolds was evaluated by rBMSCs. As shown in Figure 3a, the proliferation of rBMSCs in the 2WES-TCP scaffolds group was obviously higher than that in the TCP and 4WES-TCP scaffolds groups on day 3 and day 7. Therefore, this study selected the 2WES-TCP scaffold for further experiments. The SEM images revealed that the rBMSCs spread well on TCP and 2WES-TCP scaffolds with abundant filopodia in Figure 3b,c. Furthermore, we analyzed the effect of 2WES-TCP scaffolds on the osteogenic differentiation of rBMSCs. As shown in Figure 3d−g, compared to the pure TCP group, the expression of runt-related transcription factor 2 (Runx-2), Sox-9 gene, and Osterix (SP7) of rBMSCs in 2WES-TCP scaffolds were distinctly upregulated on day 7.

3.3. WES-TCP Composite Scaffolds Stimulating the In Vitro Proliferation of Chondrocytes. As shown in Figure 4a, it is worth noting that compared with 4WES-TCP scaffolds, 2WES-TCP scaffolds could significantly promote the proliferation of chondrocytes on day 7. We also analyzed the specified gene expression in chondrocytes cultured on 3D-printed TCP and (1, 2)WES-TCP scaffolds. As shown in Figure 4b−d, compared to the pure TCP group, the expression of COL II, SOX-9, and AGGRECAN genes in chondrocytes were distinctly upregulated. Furthermore, the CLSM and SEM images revealed that the chondrocytes on pure TCP and 2WES-TCP scaffolds spread well with abundant filopodia in Figure 4e−h.

3.4. WES-TCP Composite Scaffolds Stimulating the In Vivo Osteochondral Regeneration. We further investigated the in vivo osteochondral regenerative efficacy of 3D-printed 2WES-TCP composite scaffolds according to the rabbit osteochondral defect model. At 12 weeks postsurgery, the rabbits were executed and tissue samples were obtained for histological analysis. As shown in Figure 5a−c, V&G staining exhibited that there was more bone tissue formation in the 2WES-TCP group compared with Blank and TCP groups. The control group did not realize adequate healing of the osteochondral defect and had poor bone regeneration and large residual void spaces. Meanwhile, more positive staining for cartilaginous ECM, collagen, and cell filling was found in the 2WES-TCP scaffold group through toluidine blue staining (Figure 5d−f). The photographs of bone tissue also intuitively

https://doi.org/10.1021/acsomega.3c03284
ACS Omega 2023, 8, 37918−37926

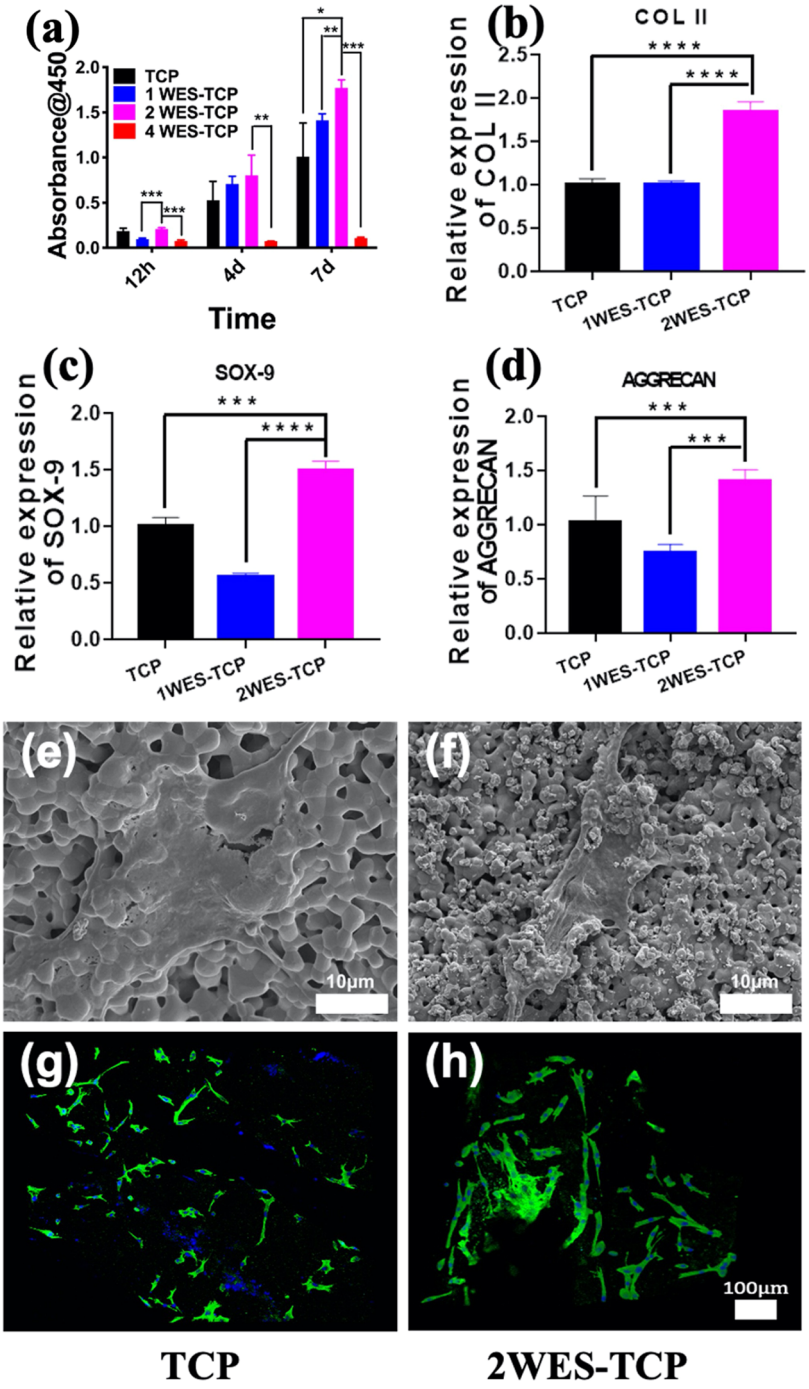

Figure 4. Proliferation and morphology of chondrocytes cultured on 3D-printed WES-TCP scaffolds. Proliferation of chondrocytes cultured on pure TCP and WES-TCP scaffolds (a). Gene expression of COL II (b), SOX-9 (d), and AGGRECAN (d) in chondrocytes after coculturing with the scaffolds for 7 d. The SEM images of chondrocytes after seeding in TCP (e) and 2WES-TCP (f) scaffolds, and confocal laser scanning microscopy (CLSM) images of chondrocytes after seeding in TCP (g) and 2WES-TCP (h) scaffolds ($n = 3$, $^{*}p < 0.05$, $^{**}p < 0.01$, $^{***}p < 0.001$, $^{****}p < 0.0001$).

displayed the cartilage repair effect at the defective sites (Figure 5g–i).

4. DISCUSSION

Recently, many studies have shown that silicate bioactive scaffolds have attracted much attention for excellent bioactivity, and could enhance bone regeneration.[22] In this study, we successfully incorporated WES into TCP bioceramics and fabricated 3D-printed porous composite scaffolds. Our results suggest that the incorporation of 2WES into 3D-printed TCP composite scaffolds significantly enhanced the bone regeneration property. In addition, the 3D printing methods are efficient in controlling the internal parameters of the porous structure such as morphology, distribution, and morphology.[23] Such a porous structure of 3D-printed scaffolds is an essential factor for guiding and stimulating the bone regeneration process, which could promote the transport of nutrition and growth of cells.

https://doi.org/10.1021/acsomega.3c03284
ACS Omega 2023, 8, 37918−37926

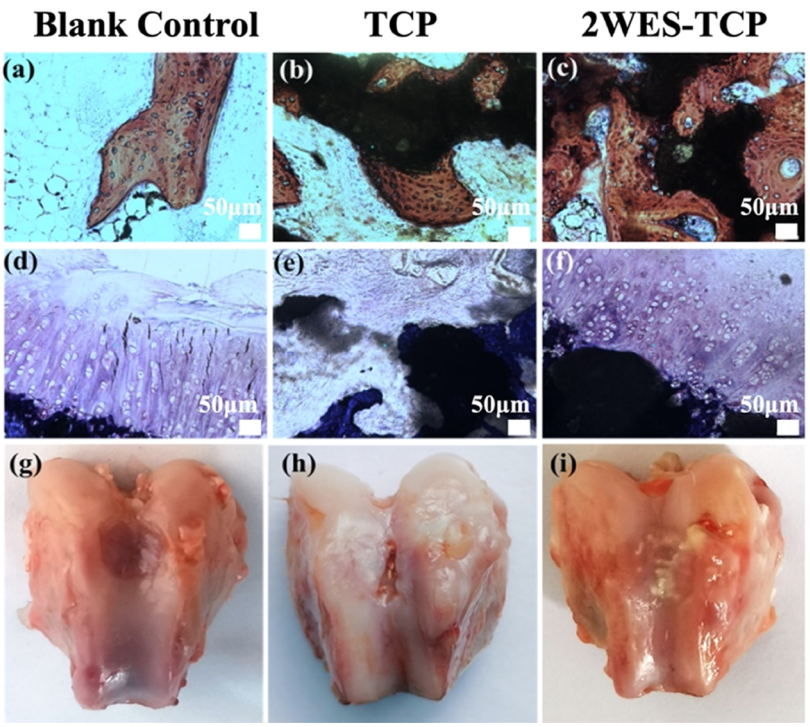

Figure 5. Regeneration quality of subchondral bone and cartilage in vivo after 12 weeks. V&G staining (a−c) and toluidine blue staining (d−f) images of tissue samples. Photographs of tissue in different groups at 12 weeks (g−i).

In this study, we found that the compressive strength and Young's moduli of 2WES-TCP scaffolds were distinctly increased. Sr element could increase the mechanical properties by providing more functional groups and promoting ions to be bonded. It was also reported that the addition of Sr ion improved the strength of scaffolds, which makes scaffolds suitable for subsequent implantations.[24] However, the mechanical properties were negatively affected by the high content of WES (4%). The compressive strength and Young's moduli of the 4WES-TCP group were significantly lower than those of the 1WES-TCP and 2WES-TCP groups may be because of the faster degradation rate of the 4WES-TCP group.[25]

The results of our study found that the synthesized WES-TCP significantly promoted the osteogenic differentiation of rBMSCs in vitro and the regeneration of subchondral bone in vivo. The results indicated that 3D-printed WES-TCP composite scaffolds have superior osteogenic bioactivity, and 2WES-TCP scaffolds possessed enhanced osteogenic performance in vitro and in vivo. The sustained release of Sr, Cu, and Si bioactive ions from 3D-printed composite scaffolds was the possible reason for the excellent bone regeneration property. The possible mechanisms are as follows. On one hand, the released Sr ions could activate the ERK-MAPK/Wnt signaling pathway to enhance bone formation.[26−29] On the other hand, the released Si ions could activate the AMPK/ERK1/2 signaling pathway, promote the osteogenic differentiation of rBMSCs, and further enhance bone formation.[30] In addition, vascularization plays an important role in the osteogenesis process via renewable autologous cells and nutrient supply.[31] The released Cu ions could stimulate the vascularization of HUVECs.[32] Based on these studies, it is reasonable to conclude that the Cu, Si, and Sr bioactive ions from 3D-printed composite scaffolds could effectively promote the regeneration of subchondral bone.

The interesting result of our study shows that 3D-printed WES-TCP composite scaffolds not only enhanced the regeneration of subchondral bone but also improved the regeneration of cartilage. The expression of the SOX-9, COL II, and AGGRECAN genes in chondrocytes was obviously elevated by the WES-TCP scaffolds. The possible reasons are as follows. First, by stimulating the expression of COL II, the SOX-9, and AGGRECAN genes, the activated HIF pathway of chondrocytes could support matrix synthesis and chondrocyte regeneration of cartilage reconstruction.[33] Additionally, the expression of the IHH gene is regulated by the hedgehog pathway and plays a vital role in OA onset and development.[34,35] Moreover, Si and Sr ions released from bioactive ceramic scaffolds could activate the HIF signal pathway to promote cartilage regeneration in vivo, stimulate chondrocyte maturation in vitro, and protect chondrocytes from OA via inhibiting the hedgehog pathway.[36] Cu, a key trace element that is an essential component in the synthesis of cellular enzymes in healthy cartilage tissues, such as lysyl oxidase, is a copper-dependent amine oxidase, a key enzyme for collagen cross-linking and could promote cartilage formation.[37−39] The released Cu ions from composite scaffolds could activate the HIF pathway and shift macrophages to an anti-inflammation M2 phenotype, which plays a vital role in promoting the differentiation of chondrocytes.[40] Hence, it implies that the synergistic effect of Sr, Cu, and Si ions from 3D-printed composite scaffolds could effectively promote the regeneration of cartilage.

Medicines are used for OA treatment in clinics, which may cause side effects, such as most medicines are smoothened antagonists that could reduce subchondral bone remolding or osteophyte overgrowth.[36] In addition, different constructs of scaffolds such as biphasic scaffolds and other multilayered scaffolds have been fabricated for reconstructing osteochondral defects. However, these strategies also have obvious

https://doi.org/10.1021/acsomega.3c03284
ACS Omega 2023, 8, 37918−37926

limitations, for example, insufficient mechanical integration between two layers, and poor biological simulation of functional and structural characteristics.[36] There are a few studies that show that monophasic scaffolds are used to restore the complex osteochondral interface microstructure and regenerate both subchondral bones and cartilage simultaneously. Herein, a monophasic WES-TCP scaffold containing multibioactive ions was successfully fabricated to repair osteochondral defects. Compared with conventional medical treatment, the prepared WES-TCP scaffolds avoided systemic toxicity. Additionally, according to the in vivo and in vitro physiological studies,[36,40] it is probable that composite WES-TCP scaffolds stimulate cartilage reconstruction and promote the regeneration of subchondral bone via the synergistic effect of the Sr, Cu, and Si ions from 3D-printed WES-TCP composite scaffolds.

5. CONCLUSIONS

In this study, WES-TCP scaffolds were successfully fabricated through the 3D printing technique. The introduction of WES enhanced the physicochemical properties of the composite scaffolds and promoted the differentiation and proliferation of rabbit BMSCs and chondrocytes. Simultaneously, the synergetic effect of Sr, Cu, and Si ions from composite scaffolds distinctly promoted the regeneration of both subchondral bones and cartilage. The related mechanisms might be that the released Cu, Sr, and Si ions possess bilineage bioactivities, which are beneficial for the regeneration of both subchondral bone and cartilage. Harnessing multibioactive ions in a monophasic scaffold offers a viable and effective strategy for the regeneration of osteochondral defects and OA therapy. The designed scaffold takes advantage of the multifunctional properties of bioceramics, which are an intelligent strategy for regenerating cartilage and subchondral bone.

■ ASSOCIATED CONTENT

Data Availability Statement

All data are available in the main text or the Supporting Information. Additional data related to this paper may be requested from the authors.

■ AUTHOR INFORMATION

Corresponding Authors

Zhenjiang Ma − *Shanghai Key Laboratory of Orthopaedic Implants, Department of Orthopaedic Surgery, Shanghai Ninth People's Hospital, Shanghai Jiao Tong University School of Medicine, Shanghai 200011, China*; Email: dr_zjma@163.com

Hui Ma − *Shanghai Key Laboratory of Orthopaedic Implants, Department of Orthopaedic Surgery, Shanghai Ninth People's Hospital, Shanghai Jiao Tong University School of Medicine, Shanghai 200011, China; Renhe Hospital, Shanghai 201900, China*; Email: orthopain@163.com

Jinwu Wang − *Shanghai Key Laboratory of Orthopaedic Implants, Department of Orthopaedic Surgery, Shanghai Ninth People's Hospital, Shanghai Jiao Tong University School of Medicine, Shanghai 200011, China*; orcid.org/0000-0003-0243-8391; Phone: +86 13301773680; Email: jinwu_wang@163.com; Fax: +86 21 63139920

Authors

Nanjian Xu − *Department of Spine Surgery, Ningbo Sixth Hospital, Ningbo, Zhejiang 32500, China*

Dezhi Lu − *Shanghai Key Laboratory of Orthopaedic Implants, Department of Orthopaedic Surgery, Shanghai Ninth People's Hospital, Shanghai Jiao Tong University School of Medicine, Shanghai 200011, China; School of Medicine, Shanghai University, Shanghai 200444, China*

Lei Qiang − *Shanghai Key Laboratory of Orthopaedic Implants, Department of Orthopaedic Surgery, Shanghai Ninth People's Hospital, Shanghai Jiao Tong University School of Medicine, Shanghai 200011, China; School of Materials Science and Engineering, Southwest Jiaotong University, Chengdu 610031, China*

Yihao Liu − *Shanghai Key Laboratory of Orthopaedic Implants, Department of Orthopaedic Surgery, Shanghai Ninth People's Hospital, Shanghai Jiao Tong University School of Medicine, Shanghai 200011, China*

Dalin Yin − *Zhejiang University of Science and Technology, Hangzhou, Zhejiang 310023, China*

Zhiyong Wang − *School of Biomedical Engineering, Shenzhen University Health Science Center, Shenzhen 518060, China*

Yongxiang Luo − *School of Biomedical Engineering, Shenzhen University Health Science Center, Shenzhen 518060, China*

Chen Yang − *Zhejiang Engineering Research Center for Tissue Repair Materials, Wenzhou Institute, University of Chinese Academy of Sciences, Wenzhou 325000, China*; orcid.org/0000-0001-9820-1692

Complete contact information is available at: https://pubs.acs.org/10.1021/acsomega.3c03284

Author Contributions

◆N.X., D.L., and L.Q. contributed equally to this work.

Notes

The authors declare no competing financial interest.

■ ACKNOWLEDGMENTS

The authors appreciate financial support from the National Key R&D Program of China (2022YFA1207500 and 2018YFA0703000), the National Natural Science Foundation of China (Grant No. 82072412/32271386), the Translation Medicine National Key Science and Technology Infrastructure (Shanghai) Open Project (TMSK-2020-118), the Lingang Laboratory "Seeking Outstanding Youth Program" Open Project (LG-QS-202206-04), the Zhejiang Province Medical and Health Science and Technology Project (No. 2022512117), the Natural Science Foundation of Ningbo City (Grant No. 202003N4299), the Ningbo Yinzhou Technology Project (2020AS0074), and the Project of Shanghai Science and Technology Commission (23ZR1447400). Table of Contents Graphic was created with BioRender.com.

■ REFERENCES

(1) Panjapheree, K.; Kamonmattayakul, S.; Meesane, J. Biphasic scaffolds of silk fibroin film affixed to silk fibroin/chitosan sponge based on surgical design for cartilage defect in osteoarthritis. *Mater. Des.* **2018**, *141*, 323−332.

(2) Hunter, D. J.; March, L.; Chew, M. Osteoarthritis in 2020 and beyond: a Lancet Commission. *Lancet* **2020**, *396*, 1711−1712.

(3) Chen, Z.; Zhang, Q.; Li, H.; Wei, Q.; Zhao, X.; Chen, F. Elastin-like polypeptide modified silk fibroin porous scaffold promotes osteochondral repair. *Bioact. Mater.* **2021**, *6*, 589−601.

(4) Khorshidi, S.; Karkhaneh, A. A review on gradient hydrogel/fiber scaffolds for osteochondral regeneration. *J. Tissue Eng. Regener. Med.* **2018**, *12*, e1974−e90.

https://doi.org/10.1021/acsomega.3c03284
ACS Omega 2023, 8, 37918−37926

(5) Urist, M. R.; Dowell, T. A.; Hay, P. H.; Strates, B. S. Inductive substrates for bone formation. *Clin. Orthop. Relat. Res.* **1968**, *59*, 59−96.
(6) Deng, C.; Chang, J.; Wu, C. Bioactive scaffolds for osteochondral regeneration. *J. Orthop. Transl.* **2019**, *17*, 15−25.
(7) Wang, S.; Duan, C.; Yang, W.; Gao, X.; Shi, J.; Kang, J.; Deng, Y.; Shi, X. L.; Chen, Z. G. Two-dimensional nanocoating-enabled orthopedic implants for bimodal therapeutic applications. *Nanoscale* **2020**, *12*, 11936−11946.
(8) Deng, Y.; Gao, X.; Shi, X. L.; Lu, S.; Chen, Z. G.; et al. Graphene Oxide and Adiponectin-Functionalized Sulfonated Poly(etheretherketone) with Effective Osteogenicity and Remotely Repeatable Photodisinfection. *Chem. Mater.* **2020**, *32*, 2180−2193.
(9) Makris, E. A.; Gomoll, A. H.; Malizos, K. N.; et al. Repair and tissue engineering techniques for articular cartilage. *Nat. Rev. Rheumatol.* **2015**, *11*, 21−34.
(10) Xu, J.; Ji, J.; Jiao, J.; Zheng, L.; Hong, Q.; Tang, H.; et al. 3D Printing for Bone-Cartilage Interface Regeneration. *Front. Bioeng. Biotechnol.* **2022**, *10*, No. 828921.
(11) Selvaggio, G.; Chizhik, A.; Nissler, R.; Kuhlemann, L.; Meyer, D.; Vuong, L.; et al. Exfoliated near infrared fluorescent silicate nanosheets for (bio)photonics. *Nat. Commun.* **2020**, *11*, No. 1495.
(12) Schumacher, M.; Gelinsky, M. Strontium modified calcium phosphate cements - approaches towards targeted stimulation of bone turnover. *J. Mater. Chem. B* **2015**, *3*, 4626−4640.
(13) Sriranganathan, D.; Kanwal, N.; Hing, K. A.; Hill, R. G. Strontium substituted bioactive glasses for tissue engineered scaffolds: the importance of octacalcium phosphate. *J. Mater. Sci.: Mater. Med.* **2016**, *27*, No. 39.
(14) Chiu, Y. C.; Shie, M. Y.; Lin, Y. H.; Lee, A. K.; Chen, Y. W. Effect of Strontium Substitution on the Physicochemical Properties and Bone Regeneration Potential of 3D Printed Calcium Silicate Scaffolds. *Int. J. Mol. Sci.* **2019**, *20*, No. 2729.
(15) Deng, C.; Zhu, H.; Li, J.; et al. Bioactive Scaffolds for Regeneration of Cartilage and Subchondral Bone Interface. *Theranostics* **2018**, *8*, 1940−1955.
(16) Yu, D.-G.; Ding, H.-F.; Mao, Y.-Q.; et al. Strontium ranelate reduces cartilage degeneration and subchondral bone remodeling in rat osteoarthritis model. *Acta Pharmacol. Sin.* **2013**, *34*, 393−402.
(17) Dong, C.; Yang, C.; Younis, M. R.; Zhang, J.; He, G.; Qiu, X.; et al. Bioactive NIR-II Light-Responsive Shape Memory Composite Based on Cuprorivaite Nanosheets for Endometrial Regeneration. *Adv. Sci.* **2022**, *9*, No. e2102220.
(18) Yang, C.; Zheng, R.; Younis, M. R.; Shao, J.; Fu, L. H.; Zhang, D. Y.; et al. NIR-II light-responsive biodegradable shape memory composites based on cuprorivaite nanosheets for enhanced tissue reconstruction. *Chem. Eng. J.* **2021**, *419*, No. 129437.
(19) Autefage, H.; Allen, F.; Tang, H. M.; Kallepitis, C.; Gentleman, E.; Reznikov, N.; et al. Multiscale analyses reveal native-like lamellar bone repair and near perfect bone-contact with porous strontium-loaded bioactive glass. *Biomaterials* **2019**, *209*, 152−162.
(20) Yang, C.; Younis, M. R.; Zhang, J.; Qu, J.; Lin, J.; Huang, P. Programmable NIR-II Photothermal-Enhanced Starvation-Primed Chemodynamic Therapy using Glucose Oxidase-Functionalized Ancient Pigment Nanosheets. *Small* **2020**, *16*, No. e2001518.
(21) Zhai, D.; Chen, L.; Chen, Y.; Zhu, Y.; Xiao, Y.; Wu, C. Lithium silicate-based bioceramics promoting chondrocyte maturation by immunomodulating M2 macrophage polarization. *Biomater. Sci.* **2020**, *8*, 4521−4534.
(22) Wang, C.; Lin, K.; Chang, J.; Sun, J. Osteogenesis and angiogenesis induced by porous beta-CaSiO(3)/PDLGA composite scaffold via activation of AMPK/ERK1/2 and PI3K/Akt pathways. *Biomaterials* **2013**, *34*, 64−77.
(23) Yang, C.; Wang, X.; Ma, B.; Zhu, H.; Huan, Z.; Ma, N.; et al. 3D-Printed Bioactive Ca3SiO5 Bone Cement Scaffolds with Nano Surface Structure for Bone Regeneration. *ACS Appl. Mater. Interfaces* **2017**, *9*, 5757−5767.
(24) Lei, Y.; Xu, Z.; Ke, Q.; Yin, W.; Chen, Y.; Zhang, C.; Guo, Y. Strontium hydroxyapatite/chitosan nanohybrid scaffolds with enhanced osteoinductivity for bone tissue engineering. *Mater. Sci. Eng.: C* **2017**, *72*, 134−142.
(25) Shie, M. Y.; Ding, S. J.; Chang, H. C. The role of silicon in osteoblast-like cell proliferation and apoptosis. *Acta Biomater.* **2011**, *7*, 2604−2614.
(26) Basu, S.; Ghosh, A.; Barui, A.; Basu, B. (Fe/Sr) Codoped Biphasic Calcium Phosphate with Tailored Osteoblast Cell Functionality. *ACS Biomater. Sci. Eng.* **2018**, *4*, 857−871.
(27) Chiu, Y. C.; Fang, H. Y.; Hsu, T. T.; Lin, C. Y.; Shie, M. Y. The Characteristics of Mineral Trioxide Aggregate/Polycaprolactone 3-dimensional Scaffold with Osteogenesis Properties for Tissue Regeneration. *J. Endod.* **2017**, *43*, 923−929.
(28) Lin, Y. H.; Chiu, Y. C.; Shen, Y. F.; Wu, Y. A.; Shie, M. Y. Bioactive calcium silicate/poly-epsilon-caprolactone composite scaffolds 3D printed under mild conditions for bone tissue engineering. *J. Mater. Sci. Mater. Med.* **2017**, *29*, No. 11.
(29) Lin, K. L.; Xia, L. G.; Li, H. Y.; Jiang, X. Q.; Pan, H. B.; Xu, Y. J.; et al. Enhanced osteoporotic bone regeneration by strontium-substituted calcium silicate bioactive ceramics. *Biomaterials* **2013**, *34*, 10028−10042.
(30) Wang, C.; Lin, K. L.; Chang, J.; Sun, J. Osteogenesis and angiogenesis induced by porous beta-CaSiO3/PDLGA composite scaffold via activation of AMPK/ERK1/2 and PI3K/Akt pathways. *Biomaterials* **2013**, *34*, 64−77.
(31) Feng, C.; Zhang, W.; Deng, C.; Li, G.; Chang, J.; Zhang, Z.; et al. 3D Printing of Lotus Root-Like Biomimetic Materials for Cell Delivery and Tissue Regeneration. *Adv. Sci.* **2017**, *4*, No. 1700401.
(32) Kong, N.; Lin, K.; Li, H.; Chang, J. Synergy effects of copper and silicon ions on stimulation of vascularization by copper-doped calcium silicate. *J. Mater. Chem. B* **2014**, *2*, 1100−1110.
(33) Bouaziz, W.; Sigaux, J.; Modrowski, D.; Devignes, C. S.; Funck-Brentano, T.; Richette, P.; et al. Interaction of HIF1alpha and beta-catenin inhibits matrix metalloproteinase 13 expression and prevents cartilage damage in mice. *Proc. Natl. Acad. Sci. U.S.A.* **2016**, *113*, 5453−5458.
(34) Zhou, J.; Chen, Q.; Lanske, B.; Fleming, B. C.; Terek, R.; Wei, X.; et al. Disrupting the Indian hedgehog signaling pathway in vivo attenuates surgically induced osteoarthritis progression in Col2a1-CreERT2; Ihhfl/fl mice. *Arthritis Res. Ther.* **2014**, *16*, No. R11.
(35) Zhang, C. M.; Wei, X. C.; Chen, C. W.; Cao, K.; Li, Y. P.; Jiao, Q.; et al. Indian Hedgehog in Synovial Fluid Is a Novel Marker for Early Cartilage Lesions in Human Knee Joint. *Int. J. Mol. Sci.* **2014**, *15*, 7250−7265.
(36) Deng, C.; Zhu, H.; Li, J.; Feng, C.; Yao, Q.; Wang, L.; et al. Bioactive Scaffolds for Regeneration of Cartilage and Subchondral Bone Interface. *Theranostics* **2018**, *8*, 1940−1955.
(37) Bost, M.; Houdart, S.; Oberli, M.; Kalonji, E.; Huneau, J. F.; Margaritis, I. Dietary copper and human health: Current evidence and unresolved issues. *J. Trace Elem. Med. Biol.* **2016**, *35*, 107−115.
(38) Alshenibr, W.; Tashkandi, M. M.; Alsaqer, S. F.; Alkheriji, Y.; Wise, A.; Fulzele, S.; et al. Anabolic role of lysyl oxidase like-2 in cartilage of knee and temporomandibular joints with osteoarthritis. *Arthritis Res. Ther.* **2017**, *19*, No. 179.
(39) Huang, Z. M.; Du, S. H.; Huang, L. G.; Li, J. H.; Xiao, L.; Tong, P. Leptin promotes apoptosis and inhibits autophagy of chondrocytes through upregulating lysyl oxidase-like 3 during osteoarthritis pathogenesis. *Osteoarthritis Cartilage* **2016**, *24*, 1246−1253.
(40) Lin, R.; Deng, C.; Li, X.; Liu, Y.; Zhang, M.; Qin, C.; et al. Copper-incorporated bioactive glass-ceramics inducing anti-inflammatory phenotype and regeneration of cartilage/bone interface. *Theranostics* **2019**, *9*, 6300−6313.

https://doi.org/10.1021/acsomega.3c03284
ACS Omega 2023, 8, 37918−37926